Theoretical studies of reaction pathways and energy barriers for alkaline hydrolysis of phosphotriesterase substrates paraoxon and related toxic phosphofluoridate nerve agents

Fang Zheng,[b] Chang-Guo Zhan*†[a] and Rick L. Ornstein[b]

[a] *Department of Medicine, College of Physicians & Surgeons, Columbia University, New York, NY 10032, USA*
[b] *Pacific Northwest National Laboratory, Mailstop K2-21, Battelle Blvd., PO Box 999, Richland, WA 99352, USA*

Received (in Cambridge, UK) 23rd February 2001, Accepted 26th September 2001
First published as an Advance Article on the web 1st November 2001

Ab initio molecular orbital calculations were carried out to study reaction pathways and evaluate energy barriers for alkaline hydrolysis of *O*,*O*-diethyl *p*-nitrophenyl phosphate (paraoxon), diisopropyl phosphorofluoridate (DFP), *O*-isopropyl methylphosphonofluoridate (sarin), *O*-pinacolyl methylphosphonofluoridate (soman) and *O*,*O*-dimethyl phosphorofluoridate. This is the first computational study on the reaction pathways for hydrolysis of phosphotriesters and their structural variants that have small pK_a values for the leaving groups. The reaction coordinate calculations reveal that the hydrolysis of DFP, sarin, soman and *O*,*O*-dimethyl phosphorofluoridate proceeds through the attack of hydroxide ion at the phosphorus center to form a pentacoordinate intermediate and the decomposition of the intermediate through F leaving. The hydrolysis of paraoxon was found to occur by a one-step process, which strongly supports the conclusion, based on the previously observed primary and secondary ^{18}O isotope effects, of an S_N2-like transition state with the absence of a stable pentacoordinate intermediate during the paraoxon hydrolysis. The energy barriers calculated in the gas phase for the pentacoordinate intermediate decomposition step are slightly lower than for the formation step for DFP and sarin, and are higher for soman and *O*,*O*-dimethyl phosphorofluoridate. Solvent effects significantly increase the energy barriers for the pentacoordinate intermediate formation step and significantly decrease the energy barriers for the decomposition step. Thus, the pentacoordinate intermediate formation step of hydrolysis in aqueous solution is always rate-determining. For the hydrolysis of all the compounds examined in this study, the energy barrier, 0.8 kcal mol^{-1}, calculated for the paraoxon hydrolysis is the lowest in the gas phase, whereas the corresponding barrier, 10.1 kcal mol^{-1}, is the highest in aqueous solution. For the hydrolysis of sarin in aqueous solution, for which the experimental activation energy is available, the calculated energy barrier of 8.6 kcal mol^{-1} for the pentacoordinate intermediate formation (*i.e.* the rate-determining step) is in good agreement with the experimental activation energy of 9.1 kcal mol^{-1}. Finally, the relative magnitudes of the energy barriers calculated for the alkaline hydrolysis were qualitatively compared with the relative magnitudes of the available experimental rate constants reported for the corresponding phosphotriesterase-catalyzed hydrolysis, and were employed to discuss substituent effects.

Introduction

The hydrolysis of phosphate esters is one of the most fundamental chemical and biochemical reactions.[1] Phosphotriesters such as *O*,*O*-diethyl *p*-nitrophenyl phosphate (paraoxon) have been widely used as agricultural insecticides. In addition to insect control, phosphotriesters can also poison mammalian systems. As a result, structural variants of phosphotriesters, such as *O*-isopropyl methylphosphonofluoridate (sarin) and *O*-pinacolyl methylphosphonofluoridate (soman), which are generally referred to as G-series nerve agents, or their surrogates such as diisopropyl fluorophosphate (DFP) have been developed as potent biological warfare nerve agents.[2]

These compounds are extremely potent inhibitors of acetylcholinesterase (AChE), the enzyme responsible for regulating the concentration of the neurotransmitter acetylcholine. If AChE activity is blocked, acetylcholine accumulates at cholinergic receptor sites, thereby excessively stimulating the cholinergic receptors. This can lead to various clinical complications including fibrillation, leading ultimately to death. Exposure to excess levels of organophosphorus compounds not only has immediate consequences but also has been shown to exert delayed cholinergic toxicity and delayed neurotoxicity.[3] Long term exposure to low levels of organophosphates can produce persistent and additive inhibition of acetylcholinesterase resulting in a delayed neuropathy.[4]

Phosphotriesters and their derivatives are toxic to both target and non-target organisms. One example is that paraoxon is also the compound most often responsible for the poisoning of agricultural workers. Interest in the efficient chemical destruction of these toxic organophosphate esters remains an active research scientific area, with attention recently focused on peroxides,[5] iodosocarboxylates,[6] metallomicelles,[7] enzymes,[8] and antibodies[9] as hydrolytic catalysts. However, the extreme toxicity of the compounds such as the phosphorus nerve agents sarin and soman *etc.* often mandates that most laboratory research employs models or simulants instead of the actual compounds. *p*-Nitrophenyl diphenylphosphate is a well-known unofficial standard simulant for hydrolytic reactions of phosphotriester.[10]

† Currently visiting at Pacific Northwest National Laboratory. E-mail: Chang-Guo.Zhan@pnl.gov

DOI: 10.1039/b101747k

As to the hydrolysis of organophosphate esters in aqueous solution, the currently dominant view is that hydrolysis of monoesters proceeds by a dissociative, unimolecular elimination pathway, whereas diesters and triesters follow a bimolecular base-catalyzed hydrolysis mechanism. The bimolecular base-catalyzed hydrolysis is initialized by attack of a nucleophile, hydroxide ion being concerned in this study, at the phosphorus atom of the ester. Analysis of experimental results suggested that reactions of nucleophiles with neutral phosphoryl species could proceed either through a two-step pathway involving a pentacoordinate intermediate or through a concerted one-step pathway when the pK_a value of the leaving group is very small.[11–13]

Based on theoretical studies of the detailed reaction pathways and the corresponding energy barriers, Florian and Warshel *et al.* recently questioned a long-standing mechanistic postulate for the phosphate monoester hydrolysis mechanism.[14] With their calculated results in mind, they reexamined the available experimental data and found that although experimental results for solution reactions had usually been considered as evidence for the dissociative pathway, a closer thermodynamic analysis of observed linear free energy relationships showed that the experimental information is consistent with the associative, concerted and dissociative alternatives.[15] Their work indicates that reliable computational studies of fundamental reaction pathways and the corresponding energetics are necessary even for chemical reactions that have been thoroughly investigated by experiments.

Although there have been some publications related to the quantum mechanical calculation of phosphate ester hydrolysis,[14,16,17] no one has addressed the hydrolysis of the toxic phosphotriesters and their structural variants. Previous computational studies of phosphotriester hydrolysis focused on trimethyl phosphate *etc.*,[17] for which the leaving group is associated with a large pK_a value. The calculations indicated that the dominant pathway for hydrolysis of those phosphate triesters involved an intramolecular proton transfer to the leaving group and that the leaving group left the phosphorus as a protonated form in the product. However, this is not the case for hydrolysis of phosphate triesters and their structural variants that have small pK_a values for the leaving groups. It is known from previous experimental studies that the hydrolysis of these phosphotriesters and their structural variants proceeds with a net inversion of stereochemistry at the phosphorus centre,[18] *i.e. via* an S_N2 type mechanism for which the attacking nucleophile (OH^- in this case) and the leaving group are positioned on opposite sides of the plane formed by the three remaining atoms attached to the phosphorus. According to this mechanism, the leaving group should leave the phosphorus as a deprotonated form in the product.

In the present work, we focus on the dominant reaction pathway for hydrolysis of phosphate triesters and their structural variants that have small pK_a values for the leaving groups. The base-catalyzed hydrolyses of paraoxon, sarin, soman, DFP and *O*,*O*-dimethyl phosphorofluoridate were studied in both the gas phase and aqueous solution. For each of these compounds, reaction coordinate calculations were carried out and were followed by self-consistent reaction field (SCRF) calculations. The substituent and solvent effects were revealed by the relative magnitudes of the energy barriers calculated at the same level of theory for all the reactions. The calculated energy barriers for the base-catalyzed hydrolysis were compared with available experimental kinetic data for the hydrolysis catalyzed by phosphotriesterase (PTE), which provides further insight into the mechanism of the PTE-catalyzed hydrolysis. Theoretical studies of the toxic phosphotriesters and structural variants would be of great value since with the clarified reaction mechanism of the hydrolysis more achievable and successful experiments can be inspired, which in turn reduces the need for experimental scientists to have contact with these toxic compounds.

Calculation methods

For the reaction of hydroxide ion with each considered molecule in the gas phase, we first employed the Hartree–Fock (HF) method with the 6-31G* basis set to search for and to fully optimize geometries of all possible transition states and intermediates as well as the reactants and products. For all systems studied, vibrational frequency calculations were carried out to confirm all the first-order saddle points and local minima on the potential energy surfaces and to evaluate the zero-point vibration energies (ZPVE). Intrinsic reaction coordinate (IRC)[19] calculations were performed to verify the expected connections of the first-order saddle points with local minima on the potential energy surface. The geometries optimized at the HF/6-31G* level of theory were further refined at the HF/6-31+G* level. The geometries optimized at the HF/6-31+G* level were employed to perform the second-order Møller–Plesset (MP2) energy calculations with the 6-31+G* basis set.

Previous theoretical studies[20a,b] of fundamental reaction pathways for base-catalyzed hydrolysis of carboxylic acid esters indicated that electron correlation effects are not important in geometry optimizations, but are important in final energy calculations, for studying energy profiles of those organic reactions. With a given basis set, the energy barriers evaluated by performing MP2 energy calculations using MP2 geometries are all very close to those evaluated by the MP2 calculations using geometries optimized with HF and density functional theory (DFT) methods. The energy barriers calculated with the MP2 method are all very close to those calculated with MP4SDQ, QCISD and QCISD(T) methods, indicating that the MP2 method is sufficiently accurate for recovery of the electron correlation. Regarding the basis set dependence, the energy barriers determined with the 6-31+G* and 6-31++G** basis sets are very close to those determined with the 6-311++G(3d,3p) basis set.[20a] To further examine the accuracy of the energy barriers calculated at the MP2/6-31+G*//HF/6-31+G* level, in the present study, the optimization of geometries and evaluation of the energy barrier for the first step of hydrolysis of *O*,*O*-dimethyl phosphorofluoridate in the gas phase were also performed at other levels of theory, including a variety of HF, DFT (using B3LYP functional), and MP2 calculations with the 6-31+G* and 6-31++G** basis sets.

Solvent shifts of the energies were accounted for by performing self-consistent reaction field (SCRF) energy calculations using the geometries optimized at the HF/6-31+G* level in the gas phase. The energy barrier in aqueous solution was taken as a sum of the energy change calculated at the MP2/6-31+G*//HF/6-31+G* level in the gas phase and the corresponding solvent shift determined by the SCRF calculations at the HF/6-31+G* level. To estimate the solvent effects on the optimized geometries for *O*,*O*-dimethyl phosphorofluoridate, we also performed geometry optimizations by using the quantum Onsager model implemented in the Gaussian98 program.[21] The cavity radii used were determined by following the standard procedure of volume calculation recommended for use in the Gaussian98 program.

The solute–solvent interaction can be divided into a long-range electrostatic interaction and short-range non-electrostatic interactions (such as cavitation, dispersion and Pauli repulsion).[22] The dominant long-range electrostatic interaction was evaluated by using the recently developed GAMESS[23] implementation of the surface and volume polarizations for electrostatics (SVPE).[24] The SVPE procedure is also known as the fully polarizable continuum model (FPCM)[20b,c,d] because it fully accounts for both surface and volume polarization effects in the SCRF calculation. Since the solute cavity surface is defined as a solute electron charge isodensity contour determined self-consistently during the SVPE iteration process, the SVPE results, converged to the exact solution of Poisson's equation with a given numerical tolerance, depend only on the contour

value at a given relative permittivity and a certain quantum chemical calculation level.[24a,d] By seeking the best overall agreement with experimental conformational free energy differences (62 experimental observations) in various polar solutes existing in various solvents, this single parameter value has been calibrated as ~ 0.001 au[24b] By seeking the best overall agreement with experimental ^{15}N NMR chemical shifts (48 experimental observations) in various polar solutes existing in various solvents, this single parameter value has been calibrated as ~ 0.002 au[24c] Nevertheless, for both the experimental conformational free energy differences and the NMR chemical shifts, the SVPE results with the 0.002 au contour are very close to the corresponding SVPE results with the 0.001 au contour. Based on the fitting process employed in the calibration,[24b] the root-mean-squares (rms) deviations of the 62 experimental values for the conformational free energy differences from the results calculated by the SVPE method using the 0.001 and 0.002 au contours are 0.096 and 0.104 kcal mol^{-1}, respectively. The root-mean-squares (rms) deviations of the 48 experimental values for the NMR chemical shifts from the results calculated by the SVPE method using the 0.001 and 0.002 au contours are 2.6 and 2.3 ppm, respectively.[24c] Obviously, the 0.001 and 0.002 au contours are all acceptable for the SVPE calculations on both kinds of properties. Recent SVPE calculations[25] on base-catalyzed hydrolysis of a series of carboxylic acid esters indicated that the energy barriers determined by the SVPE calculations using both the 0.001 and 0.002 au contours are all qualitatively consistent with the corresponding experimental activation energies. The SVPE calculations using the 0.001 au contour slightly and systematically underestimate the energy barriers, whereas the differences between values from the SVPE calculations using the 0.002 au contour and the corresponding average experimental values for the examined esters are smaller than the range of experimental values reported by different laboratories. In addition, Bentley recently employed the minimum in the electron density function between pairs of interacting molecules to estimate molecular sizes, and found that the molecular surfaces identified by such a procedure are in excellent agreement with the 0.002 au isodensity contour,[26] so, the 0.002 au contour was used in this study.

Finally, the contributions of short-range non-electrostatic interactions to the energy barriers were estimated by using the polarizable continuum model (PCM)[27] implemented in the Gaussian98 program[21] with the default choices in the program for the recommended standard parameters. The total solvent shift was a sum of the long-range electrostatic interaction contribution determined by the SVPE calculations and the total contribution of the short-range non-electrostatic interactions determined by the PCM calculations.

Unless otherwise indicated, the Gaussian94[28] and Gaussian98[21] programs were used to obtain the present results. All the calculations in this work were performed on Silicon Graphics, Inc. Origin 200 multiprocessor computers.

Results and discussion

Hydrolysis of *O*,*O*-dimethyl phosphorofluoridate in the gas phase

The main geometries optimized at the HF/6-31+G* level for stationary points involved in this reaction are depicted in Figs. 1 to 7 where key geometric parameters are indicated. HBRa depicted in Fig. 2(a) is the geometry of a hydrogen-bonded complex of reactants. HBRa involves an O···H–C type hydrogen bond discussed recently in the literature.[29] Note that throughout this paper the suffix "a" refers to *O*,*O*-dimethyl phosphorofluoridate, and letters "b" to "e" refer to the other systems discussed later. All calculated results indicate that during the hydrolysis of *O*,*O*-dimethyl phosphorofluoridate, *O*,*O*-dimethyl phosphorofluoridate and OH^- first form the stable hydrogen-bonded complex HBRa before progressing to

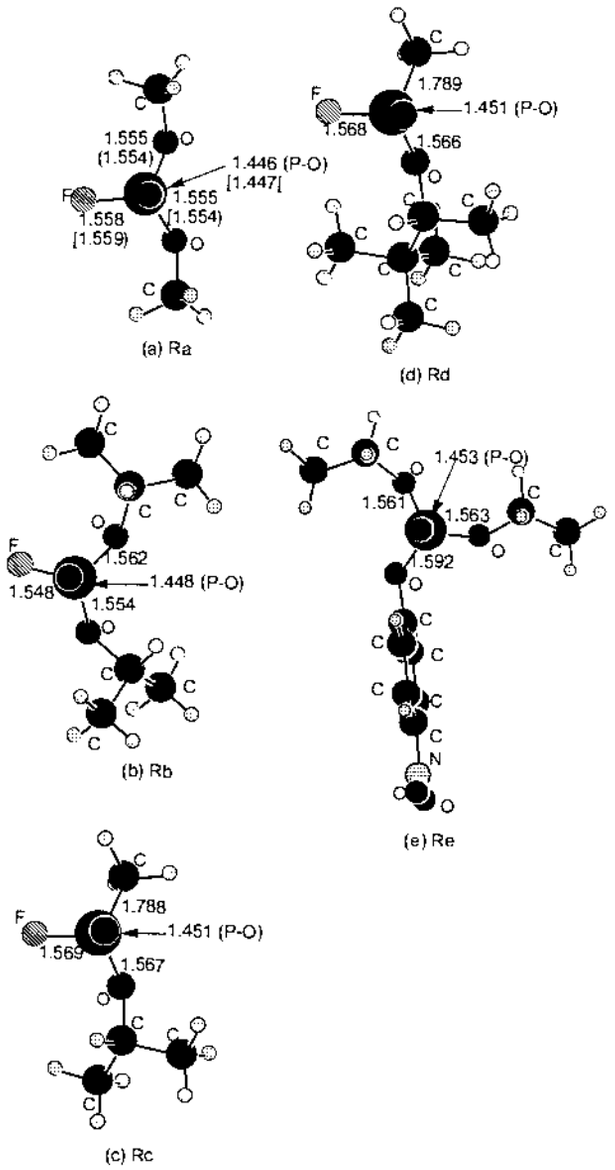

Fig. 1 Geometries of phosphofluoridates and paraoxon optimized at the HF/6-31+G* level in the gas phase. The values given in brackets are the geometric parameters optimized using the quantum Onsager model at the HF/6-31+G* level in aqueous solution.

the first transition state TS1a depicted in Fig. 3(a) and then to a pentacoordinate intermediate. Through the fluorine leaving, the pentacoordinate intermediate progresses to another transition state, TS2a, depicted in Fig. 5(a), and then to a stable hydrogen-bonded complex HBPa (not shown) between the products dimethyl phosphodiester and fluorine anion. The hydrogen bonding between the dimethyl phosphodiester and fluorine anion in HBPa is similar to that between *O*,*O*-dimethyl phosphorofluoridate and hydroxide oxygen in HBRa.

Intrinsic reaction coordinate (IRC) calculations indicate that transition states TS1a and TS2a are associated with two different conformations of the pentacoordinate intermediate. TS2a is associated with INTa depicted in Fig. 4(a), whereas TS1a is associated with INT1a depicted in Fig. 6(a). The primary difference between INT1a and TS1a lies in the orientation of two methyl groups. The methyl groups are closer to the hydroxide oxygen in INT1a and closer to fluorine in INTa. INT1a changes into INTa *via* a two-step process of conformational change corresponding to rotation about the two single P–O bonds between P and two methyloxy groups. For each step of the conformational change, rotation about one P–O bond occurs. Thus, INT1a first goes to transition state TSrot1a depicted in Fig. 6(b) and then to pentacoordinate intermediate INT2a depicted

Table 1 Energy barrier† (in kcal mol^{-1}) calculated for the pentacoordinate intermediate formation step of hydrolysis of *O*,*O*-dimethyl phosphorofluoridate in the gas phase

		Geometry optimization			
			B3LYP		
Energy calculation		HF 6-31+G*	6-31+G*	6-31++G**	MP2 6-31+G*
HF	6-31+G*	7.7	7.6		7.4
	6-31++G**		8.1	8.2	8.0
B3LYP	6-31+G*	5.4	5.3		
	6-31++G**		5.8	5.8	
MP2	6-31+G*	4.8	4.6		4.7
	6-31++G**		4.7	4.7	4.7

[a] *i.e.* The energy barrier for this reaction step is the energy change from the hydrogen-bonded complex HBRa to the first transition state TS1a.

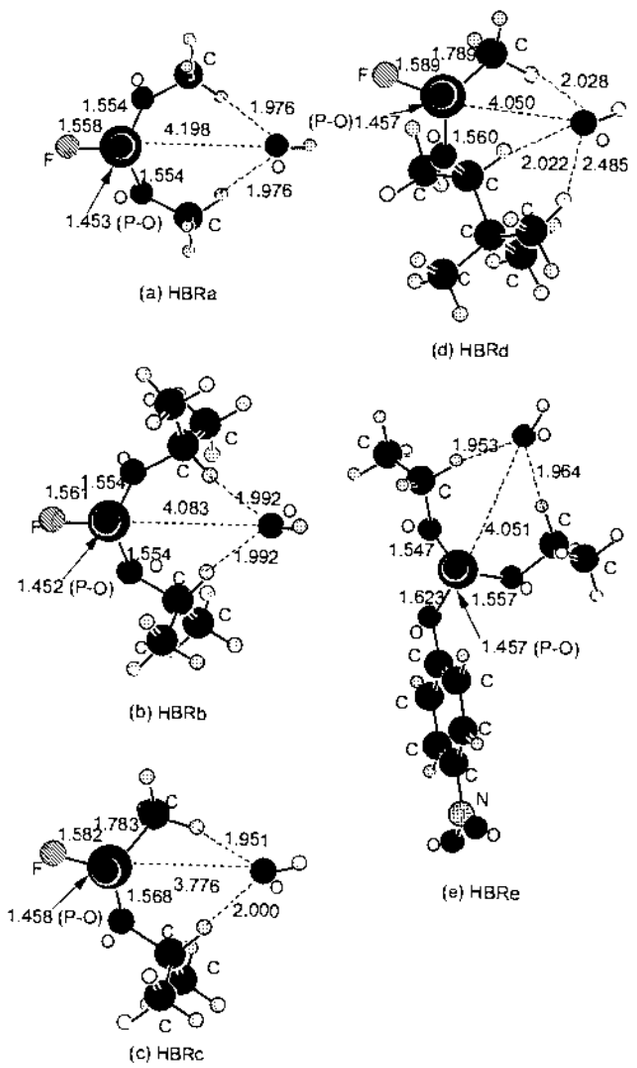

Fig. 2 Geometries of hydrogen-bonded reactant complexes optimized at the HF/6-31+G* level in the gas phase.

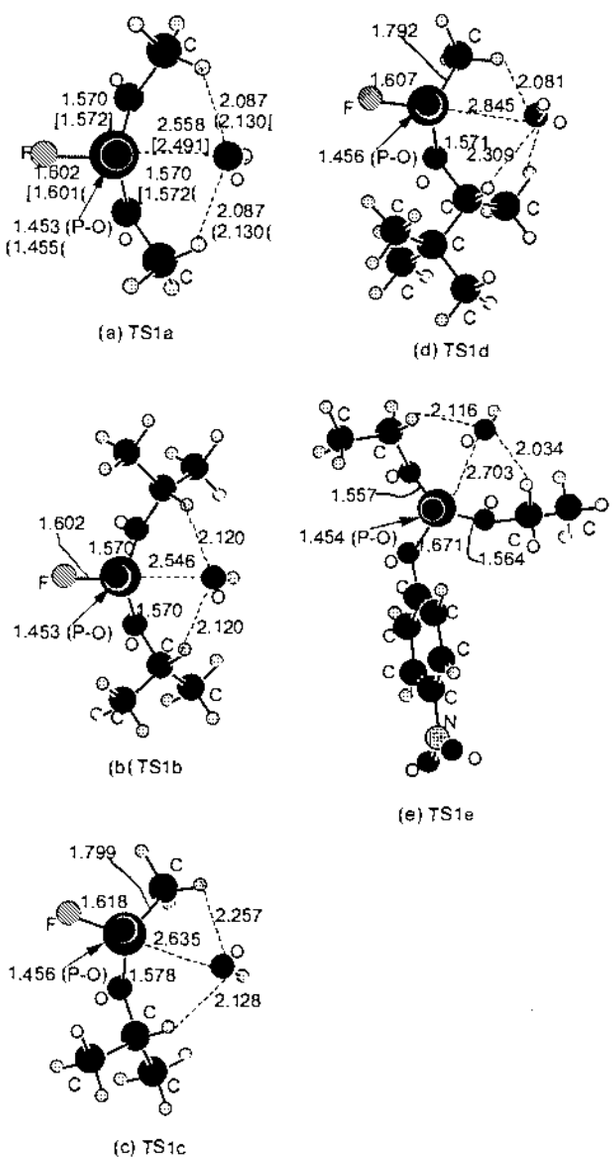

Fig. 3 Geometries of first transition states optimized at the HF/6-31+G* level in the gas phase. The values given in brackets are the geometric parameters optimized using the quantum Onsager model at the HF/6-31+G* level in aqueous solution.

in Fig. 6(c). INT2a further goes to transition state TSrot2a depicted in Fig. 6(d) and then to INTa. The two-step conformational change process is INT1a ⟶ TSrot1a ⟶ INT2a ⟶ TSrot2a ⟶ INTa. Thus, the whole hydrolysis process consists of four individual steps associated with four transition states, *i.e.* TS1a, TSrot1a, TSrot2a, and TS2a, although only the first and last steps involve chemical bond formation/breaking. The detailed energy profiles are depicted in Fig. 8.

The values of the energy barrier calculated for the first step, *i.e.* the formation of pentacoordinate intermediate INT1a, at various levels in the gas phase are summarized in Table 1 for comparison. The results calculated using geometries optimized with the HF method are all close to the corresponding results calculated using geometries optimized with the DFT and MP2 methods, indicating that electron correlation effects are indeed not important in these geometry optimizations. However, electron correlation effects on energy evaluations are significant. The energy barrier values determined by the HF method are systematically larger than the corresponding MP2 results

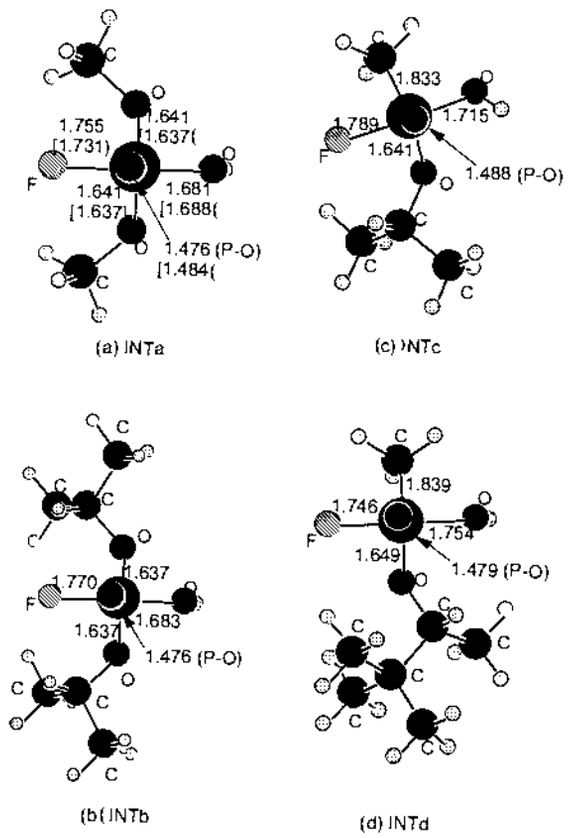

Fig. 4 Geometries of pentacoordinate intermediates corresponding to the transition states for the decomposition through P–F bond breaking optimized at the HF/6-31+G* level in the gas phase. The values given in brackets are the geometric parameters optimized using the quantum Onsager model at the HF/6-31+G* level in aqueous solution.

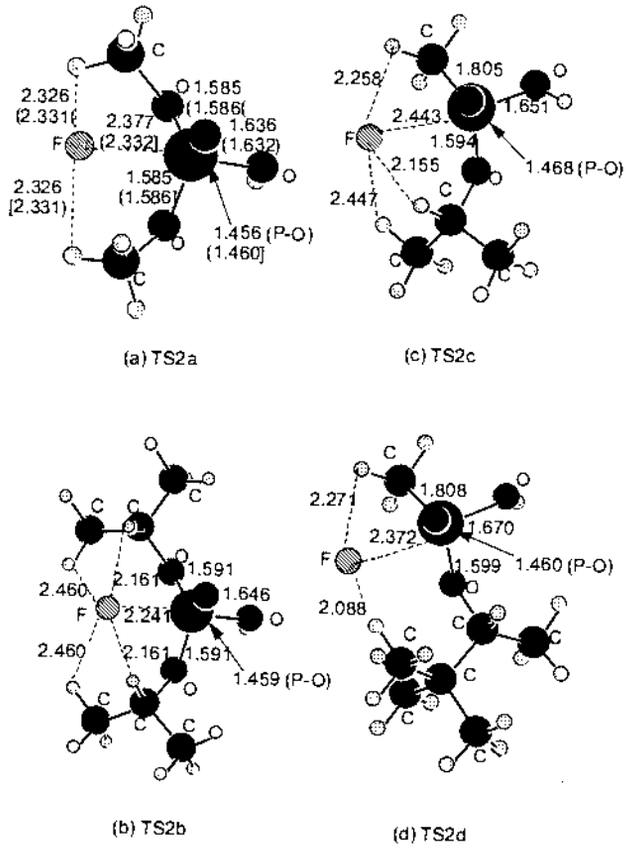

Fig. 5 Geometries of transition states for the decomposition through P–F bond breaking optimized at the HF/6-31+G* level in the gas phase. The values given in brackets are the geometric parameters optimized using the quantum Onsager model at the HF/6-31+G* level in aqueous solution.

by ~ 3 kcal mol^{-1}. The values determined by the DFT calculations are between the HF and MP2 results, and are closer to the MP2 results. Besides, the results determined by the MP2/6-31++G** calculations are very close to the corresponding results determined by the MP2/6-31+G* calculations. The energy barrier, 4.8 kcal mol^{-1}, calculated at the MP2/6-31+G*//HF/6-31+G* level is only ~ 0.1 kcal mol^{-1} larger than that calculated at the MP2/6-31+G*//MP2/6-31+G*, MP2/6-31++G**//MP2/6-31+G* and MP2/6-31++G**//B3LYP/6-31++G** levels. These results reveal that the calculations at the MP2/6-31+G*//HF/6-31+G* level are sufficient to give convincing results. Therefore, energies of all the species involved in this study were evaluated at the MP2/6-31+G*//HF/6-31+G* level of theory. The energy barriers calculated at this level for the formation and decomposition of the pentacoordinate intermediate are listed in Table 2. As seen in Table 2, the energy barrier calculated for the decomposition of pentacoordinate intermediate INTa through F leaving, is 6.2 kcal mol^{-1}, about 1.4 kcal mol^{-1} higher than that for the first step. The energy barriers calculated for the first and second steps of the conformational change are 0.1 kcal mol^{-1} (INT1a ⟶ TSrot1a) and 3.2 kcal mol^{-1} (INT2a ⟶ TSrot2a), respectively. The energy barriers for the conformational change being lower than the corresponding energy barriers for the pentacoordinate intermediate formation and decomposition is due to the fact that the conformational change does not involve any hydrogen bonding change. There is no intramolecular hydrogen bond in any of the pentacoordinate intermediates concerned in this study. Further, solvent effects significantly decrease the energy barrier for the conformational change associated with TSrot2a and significantly increase the energy barrier for the chemical bond formation step associated with TS1a (see below); the rate-determining step is always a chemical bond formation/breaking step. We therefore focus on the chemical bond formation/breaking steps in studying the hydrolysis of other compounds and in the discussion below.

In addition to the hydrolysis of *O*,*O*-dimethyl phosphorofluoridate at the P–F bond, we also examined another reaction pathway for hydrolysis at a P–O bond. The two reaction pathways share the same first reaction step, *i.e.* the formation of a pentacoordinate intermediate. The transition state geometry optimized for pentacoordinate intermediate decomposition through P–O bond breaking is TS3a, depicted in Fig. 7(b). The IRC calculation indicates that the stable conformation of pentacoordinate intermediate corresponding to TS3a is INT3a, depicted in Fig. 7(a). The energy barrier, 7.7 kcal mol^{-1}, calculated as the energy change from INT3a to TS3a, is higher than the corresponding energy barrier for pentacoordinate intermediate decomposition through P–F bond breaking. Further, solvent effects significantly increase the energy barrier for the P–O bond breaking and significantly decrease the energy barrier for the P–F bond breaking (see below); the energy barrier for the P–O bond breaking is always higher than that for the P–F bond breaking, and, therefore, the decomposition of the pentacoordinate intermediate is always dominated by the P–F bond breaking. This is consistent with the experimental observation that these kinds of compounds hydrolyze at the P–F bond and that the hydrolysis of these phosphotriesters and their structural variants proceeds with a net inversion of stereochemistry at the phosphorus centre.[18] Therefore, we focus on the P–F bond breaking pathway for hydrolysis of other phosphofluoridate compounds.

Hydrolysis of DFP, sarin and soman in the gas phase

The pentacoordinate intermediate formation and decomposition pathway found for the hydrolysis of *O*,*O*-dimethyl phosphorofluoridate at the P–F bond also exists in the

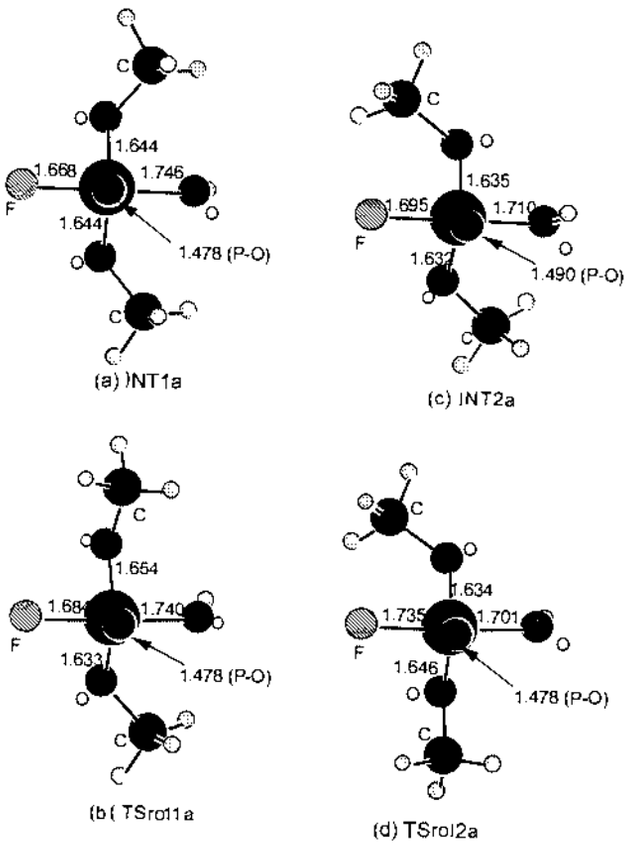

Fig. 6 Geometries of two stable conformations (INT1a and INT2a) of the pentacoordinate intermediate and the corresponding transition states (TSrot1a and TSrot2a) for the conformational change during the hydrolysis of *O*,*O*-dimethyl phosphorofluoridate optimized at the HF/6-31+G* level in the gas phase.

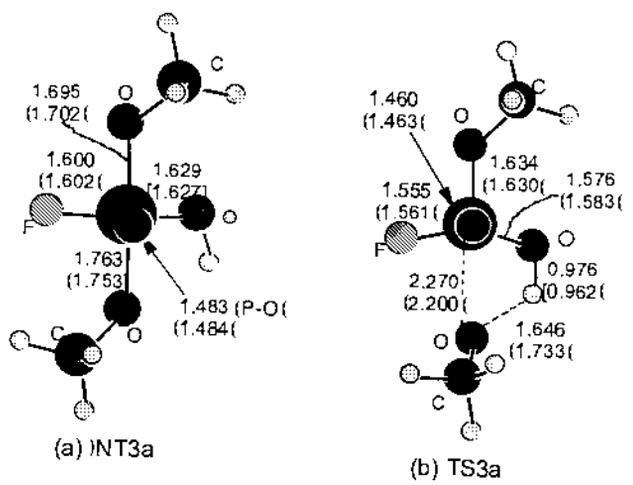

Fig. 7 Geometries of the transition state (TS3a) and the corresponding stable conformation of the pentacoordinate intermediate (INT3a) for the intermediate decomposition step of *O*,*O*-dimethyl phosphorofluoridate hydrolysis through P–O bond breaking optimized at the HF/6-31+G* level in the gas phase. The values given in brackets are the geometric parameters optimized using the quantum Onsager model at the HF/6-31+G* level in aqueous solution.

hydrolysis of DFP, sarin and soman. As shown in Table 2, the energy barriers calculated for the pentacoordinate intermediate formation step of the hydrolysis of DFP, sarin and soman are 4.5, 6.1 and 3.0 kcal mol^{-1}, respectively. The energy barriers calculated for the pentacoordinate intermediate decomposition step of the hydrolysis of DFP, sarin and soman are 3.8, 5.0 and 6.3 kcal mol^{-1}, respectively. The substituent effects on the energy barriers can be seen from comparisons between the barriers calculated for *O*,*O*-dimethyl phosphorofluoridate and

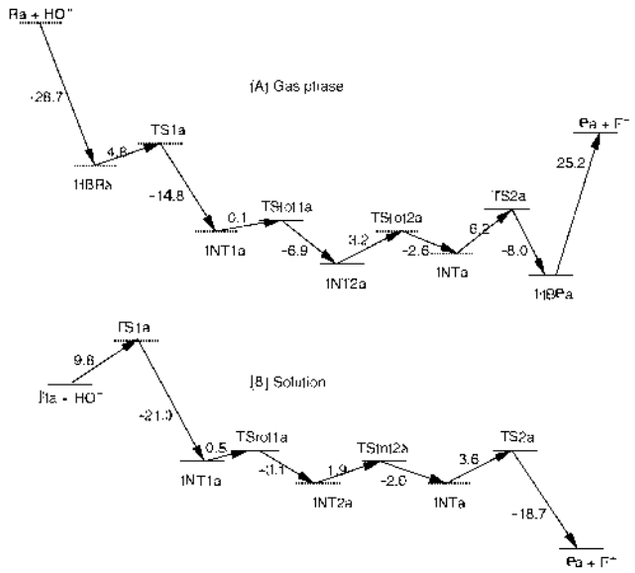

Fig. 8 Energy profiles (in kcal mol^{-1}) for the hydrolysis of *O*,*O*-dimethyl phosphorofluoridate calculated at the MP2/6-31+G*//HF/6-31+G* level in the gas phase (A) and in solution (B). Zero-point vibration energy corrections are included.

DFP and between the barriers calculated for sarin and soman. From *O*,*O*-dimethyl phosphorofluoridate to DFP, the size of the two alkyl groups becomes larger, and the energy barriers calculated for both formation and decomposition of the pentacoordinate intermediate become lower. From sarin to soman the size of one alkyl group becomes larger, and the energy barrier calculated for the pentacoordinate intermediate formation step becomes lower while the barrier calculated for the corresponding decomposition step becomes higher. Thus, the energy barriers calculated for the pentacoordinate intermediate decomposition of *O*,*O*-dimethyl phosphorofluoridate and soman are all higher than those for the corresponding formation step, whereas the energy barriers calculated for the decomposition step of DFP and sarin are all lower than those for the corresponding formation step.

Hydrolysis of paraoxon in the gas phase

The reaction pathway found for the base-catalyzed hydrolysis of paraoxon is somewhat different from the pathway found for the hydrolysis of the phosphorofluoridates and phosphonofluoridates discussed above. The route to form the transition state TS1e depicted in Fig. 3(e) is the same as that to form the first transition state TS1 for the hydrolysis of the phosphorofluoridates and phosphonofluoridates, *i.e.* during the hydrolysis paraoxon and OH^- first form a stable hydrogen-bonded complex HBRe, depicted in Fig. 2(e), before progressing to the transition state TS1e. However, the IRC calculations (using the default step size of 0.1 Å) in the forward direction indicate that the transition state TS1e directly goes to the stable hydrogen-bonded product complex HBPe, without forming a pentacoordinate intermediate and the corresponding second transition state. We also tested a geometry optimization starting from a hypothetical pentacoordinate intermediate corresponding to TS1e, and found that during the optimization process the internuclear distance between the P atom and the O atom in the leaving group became longer and longer and eventually went to HBPe. In other words, the hydrolysis of paraoxon proceeds through a one-step process in which the hydroxide attacking and leaving group leaving are concerted. Previously observed primary and secondary ^{18}O isotope effects for the base-catalyzed hydrolysis of paraoxon also provided evidence for an S_N2-like transition state with the absence of a stable pentacoordinate intermediate.[18] The calculated results strongly support the conclusion based on the experimental data. The energy

Table 2 Energy barriers (in kcal mol^{-1}) calculated at the MP2/6-31+G*//HF/6-31+G* level for the pentacoordinate intermediate formation and decomposition steps of base-catalyzed hydrolysis of phosphofluoridates and paraoxon

		a	**b**	**c**	**d**	**e**
Gas phase[b]	Formation step[c]	4.8	4.5	6.1	3.0	0.8
	Decomposition step[d]	6.2	3.8	5.0	6.3	
	Rate-determining step[e]	6.2	4.5	6.1	6.3	0.8
Aqueous solution	Formation step[f]	9.0	8.0	8.6	8.6	10.1
	Decomposition step[d]	3.6	1.8	0.3	0.7	
	Rate-determining step[e]	9.0	8.0	8.6	8.6	10.1
	Expt.[g]			9.1		

[a] **a** *O*,*O*-Dimethyl phosphorofluoridate; **b** diisopropyl phosphorofluoridate (DFP); **c** *O*-isopropyl methylphosphonofluoridate (sarin); **d** *O*-pinacolyl methylphosphonofluoridate (soman); **e** *O*,*O*-diethyl *p*-nitrophenyl phosphate (paraoxon). [b] The energies of complex-formation (*i.e.* the energy change from R to HBR) determined at the MP2/6-31+G*//HF/6-31+G* level are −28.7, −30.3, −29.2, −30.4 and −31.7 for **a**, **b**, **c**, **d** and **e**, respectively. The total energies calculated at the MP2/6-31+G*//HF/6-31+G* level are −745.17440995, −901.87150901, −748.47564840, −865.98436477, and −1233.84242493 au for **a**, **b**, **c**, **d** and **e**, respectively. The total energy calculated for HO^- at the MP2/6-31+G*//HF/6-31+G* level is −75.58778585 au. [c] The energy barrier for the pentacoordinate intermediate formation step of the hydrolysis in the gas phase is the energy change from HBR to TS1. [d] The energy barrier for the pentacoordinate intermediate decomposition step of the hydrolysis is always the energy change from INT to TS2. [e] The energy barrier for the rate-determining step is the highest one of the calculated energy barriers for hydrolysis of each compound. [f] The energy barrier for the pentacoordinate intermediate formation step of the hydrolysis in aqueous solution is the energy change from the separated reactants to TS1. [g] The experimental activation energy from ref. 31.

barrier, 0.8 kcal mol^{-1}, calculated for the hydrolysis of paraoxon in the gas phase is significantly lower than those calculated for the hydrolysis of the phosphorofluoridates and phosphonofluoridates.

Solvent effects

The geometries of Ra, HO^-, TS1a, INTa, TS2a, INT3a, and TS3a for *O*,*O*-dimethyl phosphorofluoridate hydrolyses were further optimized using the quantum Onsager model at the HF/6-31+G* level in aqueous solution. The cavity radii determined by the volume calculations are 3.98, 2.76, 4.20, 4.25, 4.16, 4.10, and 4.14 Å for Ra, HO^-, TS1a, INTa, TS2a, INT3a, and TS3a, respectively. The key geometric parameters optimized are depicted in Figs. 1, 2 to 5, and 7 for comparison with the corresponding gas phase results. As seen in the figures, the geometric parameters optimized in solution do not considerably differ from those optimized in the gas phase. The largest difference exists in transition state TS1a, depicted in Fig. 3(a), in which the internuclear distance between P and the hydroxide oxygen is about 0.067 Å. All the calculated results reveal that including the solvent effects, the total energies of the separated reactants become lower than those of the hydrogen-bonded complex HBR for each of the five compounds. Thus, in aqueous solution the separated reactants are more stable than both TS1 and HBR, while HBR is still more stable than TS1. Therefore, in aqueous solution the HBR structure is no longer associated with a local minimum on the potential energy surface, and the reaction goes directly from the separated reactants to TS1, as depicted in Fig. 8 for the hydrolysis of *O*,*O*-dimethyl phosphorofluoridate. This is because the interactions between solvent water and the separated reactants are stronger than those between the organophosphorus compound and hydroxide anion. Hence, the energy barrier for the formation of pentacoordinate intermediate in aqueous solution is the energy change from the separated reactants to the first transition state TS1. Similar results were also found for the base-catalyzed hydrolysis of carboxylic acid esters.[20a,b,d]

The energy barriers calculated using the geometries optimized in the gas phase are summarized in Table 2. The energy barrier calculated for the pentacoordinate intermediate formation step of *O*,*O*-dimethyl phosphorofluoridate hydrolysis using the geometries optimized in solution is only ~ 0.1 kcal mol^{-1} lower than the corresponding barrier of 9.0 kcal mol^{-1} calculated using the gas phase geometries, although the largest difference between gas phase and solution geometries exists in transition state TS1a associated with this reaction step. This indicates that the solvation calculations using the gas phase geometries are adequate for the reactions concerned in this study.

Including the solvent effects, the calculated energy barriers for the conformational change of the pentacoordinate intermediate associated with transition states TSrot1a and TSrot2a are 0.5 and 1.9 kcal mol^{-1}, respectively, compared to the corresponding barriers of 0.1 and 3.2 kcal mol^{-1} calculated in the gas phase. The energy barriers calculated for the conformational change are significantly lower than the barrier of 9.0 kcal mol^{-1} calculated for the formation of the pentacoordinate intermediate. The energy barrier of 10.5 kcal mol^{-1} calculated for the pentacoordinate intermediate decomposition step of *O*,*O*-dimethyl phosphorofluoridate hydrolysis at the P–O bond associated with transition state TS3a is ~ 7 kcal mol^{-1} higher than the barrier of 3.6 kcal mol^{-1} for the corresponding decomposition step of the hydrolysis at the P–F bond associated with transition state TS2a.

The results listed in Table 2 indicate that for the hydrolysis of all the compounds examined in this study the solvent effects significantly increase the energy barriers for the pentacoordinate intermediate formation step and significantly decrease the energy barriers for the decomposition step (if there is a pentacoordinate intermediate). This is because the distance between the P atom and hydroxide/fluorine anion in transition state TS1/TS2 is significantly longer than that in the corresponding pentacoordinate intermediate. Hence, the solvent accessible area of hydroxide/fluorine anion in transition state TS1/TS2 should be significantly larger than that in the intermediate while the interactions between hydroxide/fluorine anion and water are particularly strong. Therefore, the energy barriers calculated for the pentacoordinate intermediate decomposition step of hydrolysis in aqueous solution are all negligible compared to the barriers for the formation step. Thus, the pentacoordinate intermediate formation step of hydrolysis in aqueous solution is always rate-determining. The experimental primary and secondary ^{18}O isotope effects for the base-catalyzed hydrolysis of paraoxon are also consistent with the rate-limiting addition of hydroxide.[30] In addition, experimental activation energy is available for the hydrolysis of sarin in aqueous solution. Our calculated energy barrier of 8.6 kcal mol^{-1} for the pentacoordinate intermediate formation (*i.e.* the rate-determining step) of the sarin hydrolysis is in good agreement with the experimental activation energy of 9.1 kcal mol^{-1}.[31]

Furthermore, concerning the relative magnitudes of the energy barriers determined for the pentacoordinate intermediate formation step of hydrolysis of different compounds, the energy barrier, 10.1 kcal mol^{-1}, associated with paraoxon is the highest in aqueous solution although the corresponding

barrier, 0.8 kcal mol^{-1}, is the lowest in the gas phase. From *O*,*O*-dimethyl phosphorofluoridate to DFP, while the methyl groups are all replaced by the isopropyl, the calculated energy barrier for the pentacoordinate intermediate formation step of hydrolysis in aqueous solution becomes 1.0 kcal mol^{-1} lower. However, the energy barrier calculated for the pentacoordinate intermediate formation step of hydrolysis in aqueous solution does not change from sarin to soman while the isopropyl is replaced by a larger alkyl group.

Comparison with experimental results for PTE-catalyzed hydrolysis

Recently reported experimental studies, quantum chemical calculations and molecular dynamics simulations indicate that PTE-catalyzed hydrolysis of phosphotriester proceeds through the bridging hydroxide attacking the phosphorus center of the substrate.[32] So, the reaction pathway for the first step of PTE-catalyzed hydrolysis should be similar to the fundamental pathway reported in this paper for the first step of the corresponding base-catalyzed hydrolysis. The difference exists only in the chemical environment of the reaction. For the PTE-catalyzed hydrolysis the hydroxide and substrate are bound, through non-covalent bonds, to PTE in water, whereas for the base-catalyzed hydrolysis in aqueous solution the hydroxide and substrate are all surrounded by solvent water molecules. Comparison between reliable calculations on the base-catalyzed hydrolysis and the experimental data for the PTE-catalyzed hydrolysis should give some insights into the role of the enzyme.

The experimental rate constants (the turnover numbers), k_{cat}, are available for PTE-catalyzed hydrolysis of paraoxon, DFP, sarin and soman. The k_{cat} values for paraoxon, DFP, sarin and soman were reported as 3170, 465, 56 and 3 s^{-1}, respectively.[33] So, in the presence of PTE the paraoxon hydrolysis is faster than that of the other nerve agents, whereas in aqueous solution the energy barrier calculated for the paraoxon hydrolysis is higher than the others. The presence of PTE dramatically changes the relative hydrolysis rates of two different kinds of substrates. Since the insecticide paraoxon is hydrolyzed at nearly the diffusion-limited rate (k_{cat}/K_m = 6.2 × 10^7 M^{-1} s^{-1}, K_m is the Michaelis constant),[2] the energy barrier for PTE-catalyzed hydrolysis of paraoxon is expected to be very low. Hence, it is reasonable to assume that the presence of PTE lowers the energy barrier for paraoxon hydrolysis much more than those for the others. The relative rate constants for PTE-catalyzed hydrolysis of DFP and sarin are qualitatively in agreement with the relative energy barriers calculated for the corresponding base-catalyzed hydrolysis in aqueous solution. Interestingly, the relative magnitudes of the energy barriers calculated for the hydrolysis of paraoxon, DFP and sarin in the gas phase are qualitatively in agreement with the relative magnitudes of the rate constants observed for the corresponding PTE-catalyzed hydrolysis. This is because in PTE-catalyzed hydrolysis the substrate first forms a stable pre-reactive PTE–substrate complex, as indicated in the X-ray crystal structure [32*a*] with an inhibitor bound in the active site. The inhibitor bound is a structural analog of the substrate paraoxon. In the X-ray crystal structure, the internuclear distance between the bridging hydroxide oxygen and the inhibitor phosphorus is 3.6 Å, which is close to the corresponding P–O distance in HBR depicted in Fig. 2. Thus, the energy barrier for the first hydrolysis step is the energy change from the pre-reactive complex to the first transition state, which is similar to the case of the reaction with hydroxide ion in the gas phase. It is likely that the energy barriers for the PTE-catalyzed hydrolysis are closer to those for the gas phase hydrolysis or to the average values of the barriers for the hydrolysis in the gas phase and in aqueous solution. The average values of the total energy barriers for the base-catalyzed hydrolysis of paraoxon, DFP and sarin are ~ 5.5, ~ 6.3 and ~ 7.4 kcal mol^{-1}, respectively. Keep in mind that the 10-fold rate acceleration usually corresponds to an energy barrier decrease of ~ 1.4 kcal mol^{-1} at room temperature, assuming the pre-exponential factor remains a constant. The relative magnitudes of these average values are in excellent agreement with the rate constant decreasing from paraoxon to DFP and to sarin. However, the rate constant change from sarin to soman cannot fully be understood in this way. The total energy barriers calculated for base-catalyzed hydrolysis of soman in both the gas phase and aqueous solution are almost the same as those for the corresponding hydrolysis of sarin, but PTE-catalyzed hydrolysis of sarin is about 19 times faster than PTE-catalyzed hydrolysis of soman. This might be attributed to the possibility that the cavity of the PTE active site does not accommodate the larger alkyl group in soman very well.[32*d*]

Conclusion

We have performed a series of *ab initio* molecular orbital calculations to investigate reaction pathways and energy barriers for base-catalyzed hydrolysis of *O*,*O*-diethyl *p*-nitrophenyl phosphate (paraoxon), diisopropyl phosphorofluoridate (DFP), *O*-isopropyl methylphosphonofluoridate (sarin), *O*-pinacolyl methylphosphonofluoridate (soman) and *O*,*O*-dimethyl phosphorofluoridate. The reaction coordinate calculations reveal that the hydrolysis of DFP, sarin, soman and *O*,*O*-dimethyl phosphorofluoridate occurs by the attack of hydroxide ion at the phosphorus center to form a pentacoordinate intermediate and the decomposition of the pentacoordinate intermediate occurs through loss of F$^-$. For comparison, the pathways for the conformational change of the pentacoordinate intermediate and its decomposition through P–O bond breaking were also examined for *O*,*O*-dimethyl phosphorofluoridate hydrolysis. The hydrolysis of paraoxon proceeds through a one-step process, although the transition state structure is similar to those for the pentacoordinate intermediate formation step of the hydrolysis of DFP, sarin, soman and *O*,*O*-dimethyl phosphorofluoridate. The one-step pathway found in this study strongly supports the conclusion, based on the previously observed primary and secondary ^{18}O isotope effects, of an S_N2-like transition state with the absence of a stable pentacoordinate intermediate during the paraoxon hydrolysis.

The energy barriers calculated in the gas phase for the decomposition of the pentacoordinate intermediate are slightly lower than the formation step for DFP and sarin, and are higher for soman and *O*,*O*-dimethyl phosphorofluoridate. It has been shown that solvent effects have a significant impact on the reaction mechanism. Solvent effects significantly increase the energy barriers for the pentacoordinate intermediate formation step and significantly decrease the energy barriers for the decomposition step. Therefore, the energy barriers calculated for the decomposition step of hydrolysis in aqueous solution are all negligible compared to the barriers for the formation step. Thus, the pentacoordinate intermediate formation step of hydrolysis in aqueous solution is always rate-determining. For the hydrolysis of all the compounds examined in this study, the energy barrier, 0.8 kcal mol^{-1}, calculated for the paraoxon hydrolysis is the lowest in the gas phase, whereas the corresponding barrier, 10.1 kcal mol^{-1}, is the highest in aqueous solution. For the hydrolysis of sarin in aqueous solution for which experimental activation energy is available, the calculated energy barrier of 8.6 kcal mol^{-1} for the pentacoordinate intermediate formation (*i.e.* the rate-determining step) is in good agreement with the experimental activation energy of 9.1 kcal mol^{-1}.

The energy barriers calculated for the base-catalyzed hydrolysis were compared with the experimental results reported for the corresponding phosphotriesterase-catalyzed hydrolysis. The relative magnitudes of the energy barriers calculated for base-catalyzed hydrolysis of paraoxon, DFP and sarin in the gas phase are qualitatively in agreement with the

relative magnitudes of the rate constants observed for the corresponding PTE-catalyzed hydrolysis. Further numerical analysis suggests that the energy barriers for the PTE-catalyzed hydrolysis might be closer to those for base-catalyzed hydrolysis in the gas phase or to the average values of the barriers for base-catalyzed hydrolysis in the gas phase and in aqueous solution.

Acknowledgements

This work was supported partially by the Laboratory Directed Research and Development Program (LDRD) at Pacific Northwest National Laboratory. Pacific Northwest National Laboratory is a multiprogram national laboratory operated for the U.S. Department of Energy by Battelle Memorial Institute under contract DE-AC06-76RLO 1830. FZ worked at PNNL with a Faculty Fellowship administered by Associated Western Universities, Inc.

References

1 F. H. Westheimer, *Science*, 1987, **235**, 1173.
2 S.-B. Hong and F. M. Raushel, *Biochemistry*, 1999, **38**, 1159.
3 (*a*) M. B. Abou-Donia, D. G. Graham, P. R. Timmons and B. L. Reichert, *Neurotoxicology*, 1979, **1**, 425; (*b*) F. A. F. Ali and T. R. Fukuto, *J. Toxicol. Environ. Health*, 1983, **12**, 591; (*c*) R. L. Metcalf, *Neurotoxicology*, 1982, **3**, 269.
4 F. M. Williams, C. Charlton, G. E. Deblaquiere, E. Mutch, S. S. Kelly and P. G. Blain, *Hum. Exp. Toxicol.*, 1997, **16**, 67.
5 (*a*) Y.-C. Yang, F. J. Berg, L. L. Szafraniec, W. T. Beaudry, C. A. Bunton and A. Kumar, *J. Chem. Soc., Perkin Trans. 2*, 1997, 607; (*b*) S. Bhattacharya and K. Snehalatha, *J. Org. Chem.*, 1997, **62**, 2198; (*c*) J. Toullec and M. Moukawim, *Chem. Commun.*, 1996, 221; (*d*) C. A. Bunton and H. J. Foroudian, *Langmuir*, 1993, **9**, 2832; (*e*) Y.-C. Yang, L. L. Szafraniec, W. T. Beaudry and C. A. Bunton, *J. Org. Chem.*, 1993, **58**, 6964.
6 (*a*) R. A. Moss, A. T. Kotchevar, B. D. Park and P. Scrimin, *Langmuir*, 1996, **12**, 2200; (*b*) R. A. Moss and S. Bose, *Tetrahedron Lett.*, 1997, **38**, 965; (*c*) F. J. Berg, R. A. Moss, Y.-C. Yang and H. Zhang, *Langmuir*, 1995, **11**, 411; (*d*) R. A. Moss, K. Bracken and T. J. Emge, *J. Org. Chem.*, 1995, **60**, 7739; (*e*) R. A. Moss, S. Bose, K. G. Ragunathan, N. Jayasuriya and T. J. Emge, *Tetrahedron Lett.*, 1998, **39**, 347.
7 (*a*) P. Scrimin, G. Ghirlanda, P. Tecilla and R. A. Moss, *Langmuir*, 1996, **12**, 6235; (*b*) E. Kimura, H. Hashimoto and T. Koike, *J. Am. Chem. Soc.*, 1996, **118**, 10963; (*c*) J. G. J. Weijnen and J. F. Engbersen, *Recl. Trav. Chim. Pays-Bas*, 1993, **112**, 351; (*d*) S. H. Gellman, R. Petter and R. Breslow, *J. Am. Chem. Soc.*, 1986, **108**, 2388; (*e*) F. M. Menger, L. H. Gan, E. Johnson and H. D. Durst, *J. Am. Chem. Soc.*, 1987, **109**, 2800.
8 (*a*) J. L. Vanhooke, M. W. Benning, F. M. Raushel and H. M. Holden, *Biochemistry*, 1996, **35**, 6020; (*b*) M. W. Benning, J. M. Kuo, F. M. Raushel and H. M. Holden, *Biochemistry*, 1994, **33**, 15001.
9 (*a*) D. P. Weiner, T. Weimann, M. M. Wolfe, P. Wentworth and K. D. Janda, Jr., *J. Am. Chem. Soc.*, 1997, **119**, 4088; (*b*) B. J. Lavey and K. D. Janda, *J. Org. Chem.*, 1996, **61**, 7633; (*c*) J. S. Rosenblum, L.-C. Lo, T. Li, K. D. Janda and R. A. Lerner, *Angew. Chem., Int. Ed. Engl.*, 1995, **34**, 2275.
10 (*a*) C. A. Bunton and L. Robinson, *J. Org. Chem.*, 1969, **34**, 773; (*b*) R. A. Moss and Y. Ihara, *J. Org. Chem.*, 1983, **48**, 588.
11 (*a*) F. H. Westheimer, *Chem. Rev.*, 1981, **4**, 313; (*b*) A. C. Hengge and W. W. Cleland, *J. Am. Chem. Soc.*, 1990, **112**, 7421.
12 S. J. Admiraal and D. Herschlag, *Chem. Biol.*, 1995, **2**, 729.
13 K. A. Maegley, S. J. Admiraal and D. Herschlag, *Proc. Natl. Acad. Sci. U. S. A.*, 1996, **93**, 8160.
14 J. Florian and A. Warshel, *J. Am. Chem. Soc.*, 1997, **119**, 5473.
15 J. Aqvist, K. Kolmodin, J. Florian and A. Warshel, *Chem. Biol.*, 1999, **6**, R71.
16 C.-H. Hu and T. Brinck, *J. Phys. Chem. A*, 1999, **103**, 5379.
17 (*a*) J. Florian and A. Warshel, *J. Phys. Chem. B*, 1998, **102**, 719; (*b*) N.-Y. Chang and C. Lim, *J. Phys. Chem. A*, 1997, **101**, 8706; (*c*) N.-Y. Chang and C. Lim, *J. Am. Chem. Soc.*, 1998, **120**, 2156.
18 W. E. Lewis, W. J. Donarski, J. R. Wild and F. M. Raushel, *Biochemistry*, 1988, **27**, 1591.
19 (*a*) C. Gonzalez and H. B. Schlegel, *J. Chem. Phys.*, 1989, **90**, 2154; (*b*) C. Gonzalez and H. B. Schlegel, *J. Phys. Chem.*, 1990, **94**, 5523.
20 (*a*) C.-G. Zhan, D. W. Landry and R. L. Ornstein, *J. Am. Chem. Soc.*, 2000, **122**, 1522; (*b*) C.-G. Zhan, D. W. Landry and R. L. Ornstein, *J. Am. Chem. Soc.*, 2000, **122**, 2621; (*c*) C.-G. Zhan, S. Niu and R. L. Ornstein, *J. Chem. Soc., Perkin Trans. 2*, 2001, 23; (*d*) C.-G. Zhan and D. W. Landry, *J. Phys. Chem. A*, 2001, **105**, 1296.
21 M. J. Frisch, G. W. Trucks, H. B. Schlegel, G. E. Scuseria, M. A. Robb, J. R. Cheeseman, V. G. Zakrzewski, J. A. Montgomery, R. E. Stratmann, J. C. Burant, S. Dapprich, J. M. Millam, A. D. Daniels, K. N. Kudin, M. C. Strain, O. Farkas, J. Tomasi, V. Barone, M. Cossi, R. Cammi, B. Mennucci, C. Pomelli, C. Adamo, S. Clifford, J. Ochterski, G. A. Petersson, P. Y. Ayala, Q. Cui, K. Morokuma, D. K. Malick, A. D. Rabuck, K. Raghavachari, J. B. Foresman, J. Cioslowski, J. V. Ortiz, B. B. Stefanov, G. Liu, A. Liashenko, P. Piskorz, I. Komaromi, R. Gomperts, R. L. Martin, D. J. Fox, T. Keith, M. A. Al-Laham, C. Y. Peng, A. Nanayakkara, C. Gonzalez, M. Challacombe, P. M. W. Gill, B. Johnson, W. Chen, M. W. Wong, J. L. Andres, A. C. Gonzalez, M. Head-Gordon, E. S. Replogle and J. A. Pople, Gaussian 98, Revision A.6, Gaussian, Inc., Pittsburgh PA, 1998.
22 (*a*) J. Tomasi and M. Persico, *Chem. Rev.*, 1994, **94**, 2027; (*b*) C. J. Cramer and D. G. Truhlar, in *Solvent Effects and Chemical Reactions*, O. Tapia, J. Bertran, Eds., Kluwer, Dordrecht, 1996, p. 1; (*c*) C. J. Cramer and D. G. Truhlar, *Chem. Rev.*, 1999, **99**, 2161; (*d*) D. M. Chipman, *J. Chem. Phys.*, 1997, **106**, 10194; (*e*) D. M. Chipman, *J. Chem. Phys.*, 1999, **110**, 8012; (*f*) D. M. Chipman, *J. Chem. Phys.*, 2000, **112**, 5558.
23 M. W. Schmidt, K. K. Baldridge, J. A. Boatz, S. T. Elbert, M. S. Gordon, J. H. Jensen, S. Koseki, N. Matsunaga, K. A. Nguyen, S. J. Su, T. L. Windus, M. Dupuis and J. A. Montgomery, *J. Comput. Chem.*, 1993, **14**, 1347.
24 (*a*) C.-G. Zhan, J. Bentley and D. M. Chipman, *J. Chem. Phys.*, 1998, **108**, 177; (*b*) C.-G. Zhan and D. M. Chipman, *J. Chem. Phys.*, 1998, **109**, 10543; (*c*) C.-G. Zhan and D. M. Chipman, *J. Chem. Phys.*, 1999, **110**, 1611; (*d*) Regarding the detail of the SVPE computation on a given solute under a given quantum mechanical approximation level, once the solute cavity is defined and the relative permittivity is known, the accuracy of the SVPE numerical computation depends only on the number of surface nodes (N) representing the cavity surface and the number of layers (M) describing the volume polarization charge distribution within a certain, sufficiently large three-dimensional space outside the solute cavity. If one could use an infinite number of nodes and an infinite number of layers, then the numerical results obtained from the SVPE computation would be exactly the same as those determined by the exact solution of the Poisson's equation for describing the solvent polarization potential. We have shown that the accuracy of the SVPE numerical computations employed in this study with $N = 590$ and $M = 40$ (for a step of 0.3 Å) is higher than what is required for listing in Table 2 in this paper. The relative permittivity of water used for the SVPE calculations is 78.5.
25 C.-G. Zhan, D. W. Landry and R. L. Ornstein, *J. Phys. Chem. A*, 2000, **104**, 7672.
26 J. Bentley, *J. Phys. Chem. A*, 1998, **102**, 6043.
27 (*a*) S. Miertus, E. Scrocco and J. Tomasi, *Chem. Phys.*, 1981, **55**, 117; (*b*) S. Miertus and J. Tomasi, *Chem. Phys.*, 1982, **65**, 239; (*c*) M. Cossi, V. Barone, R. Cammi and J. Tomasi, *Chem. Phys. Lett.*, 1996, **255**, 327.
28 M. J. Frisch, G. W. Trucks, H. B. Schlegel, P. M. W. Gill, B. G. Johnson, M. A. Robb, J. R. Cheeseman, T. Keith, G. A. Petersson, J. A. Montgomery, K. Raghavachari, M. A. Al-Laham, V. G. Zakrzewski, J. V. Ortiz, J. B. Foresman, J. Cioslowski, B. B. Stefanov, A. Nanayakkara, M. Challacombe, C. Y. Peng, P. Y. Ayala, W. Chen, M. W. Wong, J. L. Andres, E. S. Replogle, R. Gomperts, R. L. Martin, D. J. Fox, J. S. Binkley, D. J. Defrees, J. Baker, J. P. Stewart, M. Head-Gordon, C. Gonzalez and J. A. Pople, Gaussian 94, Revision D.1, Gaussian, Inc., Pittsburgh PA, 1995.
29 (*a*) Y. Gu, T. Kar and S. Scheiner, *J. Am. Chem. Soc.*, 1999, **121**, 9411; (*b*) E. S. Meadows, S. L. De Wall, L. J. Barbour, F. R. Fronczek, M.-S. Kim and G. W. Gokel, *J. Am. Chem. Soc.*, 2000, **122**, 3325; (*c*) R. Vargas, J. Garza, D. A. Dixon and B. P. Hay, *J. Am. Chem. Soc.*, 2000, **122**, 4750.
30 S. R. Caldwell and F. M. Raushel, *Biochemistry*, 1991, **30**, 7444.
31 L. Larsson, *Acta Chem. Scand.*, 1957, **11**, 1131.
32 (*a*) J. L. Vanhooke, M. M. Benning, F. M. Raushel and H. M. Holden, *Biochemistry*, 1996, **35**, 6020; (*b*) S.-B Hong and F. M. Raushel, *Biochemistry*, 1999, **38**, 1159; (*c*) C.-G. Zhan, O. Norberto de Souza, R. Rittenhouse and R. L. Ornstein, *J. Am. Chem. Soc.*, 1999, **121**, 7279; (*d*) J. Koca, C.-G. Zhan, R. C. Rittenhouse and R. L. Ornstein, *J. Am. Chem. Soc.*, 2001, **123**, 817.
33 K. Lai, N. J. Stolowich and J. R. Wild, *Arch. Biochem. Biophys.*, 1995, **318**, 59.